

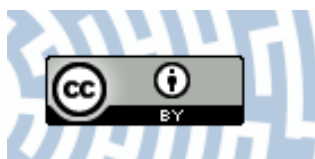


You have downloaded a document from
RE-BUS
repository of the University of Silesia in Katowice

Title: The composition induced crossover in nonlinear dielectric response in (1-x) Pb(Zr_{0.70}Ti_{0.30})O_{3-x} BiMn₂O₅ (x=0, 0.02, 0.055, 0.11, 0.15, 0.22, and 1) ceramics

Author: Seweryn Miga, Andrzej Molak, Katarzyna Balin

Citation style: Miga Seweryn, Molak Andrzej, Balin Katarzyna. (2020). The composition induced crossover in nonlinear dielectric response in (1-x) Pb(Zr_{0.70}Ti_{0.30})O_{3-x} BiMn₂O₅ (x=0, 0.02, 0.055, 0.11, 0.15, 0.22, and 1) ceramics. "Journal of Electroceramics" (2020) (online first), doi 10.1007/s10832-020-00204-9



Uznanie autorstwa - Licencja ta pozwala na kopiowanie, zmienianie, rozprowadzanie, przedstawianie i wykonywanie utworu jedynie pod warunkiem oznaczenia autorstwa.



UNIwersYTET ŚLĄSKI
W KATOWICACH



Biblioteka
Uniwersytetu Śląskiego



Ministerstwo Nauki
i Szkolnictwa Wyższego



The composition induced crossover in nonlinear dielectric response in $(1 - x) \text{Pb}(\text{Zr}_{0.70}\text{Ti}_{0.30})\text{O}_3 - x \text{BiMn}_2\text{O}_5$ ($x = 0, 0.02, 0.055, 0.11, 0.15, 0.22$, and 1) ceramics

S. Miga¹ · A. Molak² · K. Balin²

Received: 26 July 2018 / Accepted: 8 March 2020
© The Author(s) 2020

Abstract

Ceramics based on lead zirconate-titanate $\text{Pb}(\text{Zr}_{0.70}\text{Ti}_{0.30})\text{O}_3$ (PZT), bismuth manganite (BM) and the composite $(1 - x)$ PZT- x BM were obtained. A systematic study of linear and nonlinear dielectric susceptibilities temperature and frequency dependences was conducted. A composition-induced crossover in nonlinear dielectric susceptibility was detected. The so-called scaled nonlinear susceptibility, a_3 , was obtained from experimental values of the real part of the linear and third-order nonlinear dielectric susceptibilities. The value for a_3 was negative for low BM content in the whole temperature range specific to discontinuous ferroelectric phase transitions and relaxor behavior. In contradiction, a_3 was positive for BM and for the composite with sufficiently high BM content. The positive a_3 was attributed to a subsystem of dipoles created by trapped charges. Hopping charge transfer, which is a dominant mechanism for conduction in manganites, is responsible for the positive a_3 and for the colossal magnitude of the imaginary part of the linear dielectric susceptibility. The concentration of the ions was determined using scanning electron microscopy. The chemical disorder and the precipitation of ions determined using time of flight-secondary ion mass spectrometry correspond to a crossover in the electrical features.

Keywords Nonlinear dielectric properties · PZT- bismuth manganite ceramics · Phase transition · Ferroelectric relaxor

1 Introduction

Lead zirconate titanate ceramics (PZT), showing a high degree of disorder in the Zr/Ti sublattice, are piezoelectric and ferroelectric (FE) materials, which are widely applied and studied to improve their characteristics [1]. The values for the piezoelectric coefficients and dielectric losses depend on the concentration of defects, i.e., oxygen vacancies and doped ions. The $\text{Pb}(\text{Zr}_{0.70}\text{Ti}_{0.30})\text{O}_3$ (PZT 70/30) exhibits thermally activated conductivity with activation energy $E_a = 0.8$ eV [2]. This value is much lower than the energy gap, 3.0 ± 0.5 eV, estimated from XPS [3], and the 2.1 eV obtained from DOS calculation [4]. Note that oxygen vacancies, which contribute to electrical conductivity, are beyond the scope of XPS testing

and were not taken into account in the DOS calculation. The occurrences of acceptor-type doping ions, e.g., Mn^{3+} and the Ti^{3+} or Zr^{3+} ions with an induced valence, +3, stabilize oxygen vacancies, V_{O} [5, 6]. It has been proved that Mn ions substitute Zr/Ti ions [7–10]. Slight doping of PZT with 3d metals, e.g., 1 at% of Mn ions, improves the electromechanical characteristics. Bismuth manganite introduced into PZT 70/30 ceramics increased the disorder in the Zr/Ti sublattice and induced disorder in the Pb sublattice. Additionally, in the $(1 - x) \text{Pb}(\text{Zr}_{0.70}\text{Ti}_{0.30})\text{O}_3 - x \text{BiMn}_2\text{O}_5$ ($(1-x)$ PZT- x BM) compound, when the BM content was increased to $x = 0.22$, the E_a of the electric conductivity decreased to 0.37 eV and the conductivity increased by five orders of magnitude [3].

An X-ray diffraction test determined that the $(1-x)$ PZT- x BM, for $x = 0.02, 0.055, 0.11, 0.15$, and 0.22, was a composite material [2]. One phase was formed by PZT doped with Bi and Mn ions. The second phase was dominated by the BiMn_2O_5 compound with the addition of the Pb, Zr, and Ti ions. The PZT-based component showed rhombohedral non-centrosymmetric $R3m$ symmetry [11, 12]. The BiMn_2O_5 -based component exhibited orthorhombic centrosymmetric $Pbam$ symmetry. The BiMn_2O_5 structure consisted of Mn^{3+}O_5 square pyramids and Mn^{4+}O_6 octahedrons [2,

✉ S. Miga
seweryn.miga@us.edu.pl

¹ Institute of Material Science, University of Silesia, ul. 75 Pułku Piechoty 1, 40-500 Chorzów, Poland

² Institute of Physics, University of Silesia, ul. 75 Pułku Piechoty 1, 40-500 Chorzów, Poland

13–15]. The XRD measurement showed that in the 0.98 PZT–0.02 BM, a phase transition occurs between two FE rhombohedral phases with point group symmetries of $R3c$ and $R3m$ [3]. Hence, the sequence of phases was the same as that reported for pure PZT 70/30 [16]. However, the XRD test was not univocal for the other $(1-x)$ PZT– x BM composites ($x = 0.055, 0.11, 0.15, \text{ and } 0.22$). It was possible to fit the XRD pattern to either $R3c$ or $R3m$ symmetry, with similar accuracy over a wide temperature range, 290–500 K. Therefore, two possibilities were permissible: either a sequence of two FE phases or one only FE phase occurred without a phase transition occurring in these compounds [3].

The microscopic structure of several ceramic compositions from the $(1-x)$ PZT– x BM series has been studied. Those with $x = 0, 0.055, 0.11$ have been studied using the SEM test [2]. The samples showed porosity. The average chemical compositions of the studied compounds were close to nominal ones. The SIMS test has been conducted for $x = 0, 0.055, 0.11, 0.15, \text{ and } 0.22$ [3]. The PZT ceramics were homogeneous. However, in the $(1-x)$ PZT– x BM compounds, the Pb, Ti, and Mn ions exhibited a tendency to separate, whereas the Bi and Zr were distributed almost uniformly. The Vegard's law was fulfilled; hence, both the PZT-based and the BM-based phases were mutually doped. It was deduced that a composite of the two solid solutions was formed and that the ions, which substituted for each other, were distributed randomly. In such a case, these Bi^{3+} ions, which replaced Pb^{2+} ions, $\text{Bi}^{3+}_{\text{Pb}}$, induced change in valence of the Ti, Zr and $\text{Mn}_{\text{Zr/Ti}}$ ions. Such a valence change enabled charge transfer. Therefore, the heterovalent ions could form complexes with adjacent oxygen vacancies, which provided dipole-like defects [2, 3].

The Curie-Weiss anomaly related to the ferroelectric-paraelectric phase transition was clearly visible in the pure PZT 70/30 samples [2]. It was covered by an additional charge transfer contribution to the measured permittivity in the cases of 0.945 PZT–0.055 BM and 0.89 PZT–0.11 BM ceramics. These PZT–BM exhibited two frequency-dependent anomalies in permittivity. The first one occurred in the high temperature range. This anomaly has been interpreted in terms of relaxor-like features [2]. The second was a step-like anomaly that occurred in the low temperature range. This was assigned to charge transfer between the metal ions of the B sublattice of the perovskite structure. Such a charge transfer was reported for the $\text{Ti}^{3+}/\text{Ti}^{4+}$ and $\text{Mn}^{3+}/\text{Mn}^{4+}$ ions. This corresponds to dipoles created by the Ti^{3+} ions and ionized V_{O} vacancies and to a polaronic mechanism for the electric transport [17]. The effective giant dielectric permittivity of the $(1-x)$ PZT– x BM solid solution, measured at radio frequencies, may correspond to a charge transfer process. This process is related to polaron hopping and to the movement of ionic vacancies [18–20]. The relatively low activation energy related to the electronic structure of the $3d$ metal ions enabled this charge transfer effect [21, 22].

Note that conventional high-temperature sintering of bismuth manganite in air at ambient pressure resulted in the creation of two equilibrium nonpolar phases: $\text{Bi}_{12}\text{MnO}_{20}$ and BiMn_2O_5 [23–25]. Bismuth manganite ceramics showed high electrical conductivity. The small polaron hopping model was attributed to the electrical conductivity of this self-composite [15]. The activation energy increased from $E_a = 0.13$ eV below room temperature to 0.84 eV at $\sim 500\text{--}550$ K [26, 27]. The occurrence of relaxor features was assigned to the BM-originated phase in the 0.89 PZT–0.11 BM ceramics [2].

The experiments, which were conducted in the 0.1 Hz – 1 MHz frequency range, allowed one to assign a response both to the polaronic and ionic effects. When polarons hop between localized positions in the crystal lattice, they participate in the effective dielectric response. Moreover, they induce dipolar effects [28]. The localized hopping motion can be related both to the polaronic relaxation and/or dipolar relaxation [29–31]. The dipolar relaxation ought to be attributed to the occurrence of reorientable dipoles, which can originate from lattice defects or impurities. The PZT–BM ceramics studied herein also show lattice defects because of the evaporation of the lead oxide and bismuth oxide that is hardly avoided at high-temperature sintering [2, 8, 25, 27]. The other possible origin of the dipoles can be related to the movement or hopping of ions [32]. Oxygen vacancies provide the background for oxygen ions hopping at high temperatures. The hopping of oxygen ions in the perovskite structure proceeds to nearest-neighbor vacancies. Within such defected structures, the B-sublattice ions can jump into a B-sublattice vacancy, V_{B} , which is placed in the next-nearest-neighbor site [33]. The concepts of mismatch and relaxation [34] and the migration model [35] were developed from jump models, where the ions hop over a barrier back and forth between nearby vacant sites [36].

The nonlinear dielectric susceptibility is sensitive not only to the features of the phase transition but also to the induced structural disorder. The real part of the linear, second-order, and third-order dielectric susceptibilities (χ_1' , χ_2' , and χ_3' , respectively) reads as [37]:

$$P = \varepsilon_0(\chi_1'E + \chi_2'E^2 + \chi_3'E^3 + \dots) \quad (1)$$

where P is the polarization and E is the electric field. The thermodynamic consideration implies negative values of the third-order dielectric susceptibility within the paraelectric (PE) phase and positive values in the FE phase for a continuous FE–PE phase transition. Hence, it changes sign at the phase transition point [38]. In contrast, for the discontinuous FE phase transition, the χ_3' is positive within both phases, i.e., a change in the sign of χ_3' does not appear in this case. The anomalies in the nonlinear dielectric characteristics can correspond not only to FE phase transitions but also to relaxor behavior [39]. The nonlinear features may also occur in non-ferroic systems. One notices that the anisotropy of the material polarizability is

sufficient for the occurrence of a nonlinear dielectric response [37]. For example, the presence of movable dipole moments, μ , leads to the occurrence of nonzero χ_3' [40]:

$$\chi_3' = -\frac{N\mu^4}{45\varepsilon_0(k_B T)^3} \quad (2)$$

where N is the number density of dipoles, k_B is the Boltzmann constant, and T is temperature. This relation describes both the permanent molecular dipole case [37] and the case of dipole created by charge trapped in double well potential [40]. The χ_3' value, given by Eq. (2), is always negative. However, its magnitude depends on the temperature in accordance with the T^3 term, on the concentration of the dipoles and on the magnitude of the dipole moment μ .

One introduces a so-called scaled nonlinear susceptibility, a_3 , for describing nonlinear features, over a full temperature range, for various kinds of materials [41]:

$$a_3 = -\frac{\chi_3'}{\varepsilon_0^3 \chi_1'^4} \quad (3)$$

In the case of classic ferroelectrics, within the PE phase, a_3 equals to the nonlinearity coefficient B . This coefficient occurs in the thermodynamic equation of state $E = A P + B P^3$ [42]. According to Eq. (3), the sign of a_3 is opposite to the sign of χ_3' . Hence, for the continuous PE-FE phase transition, the sign of a_3 should be positive within the PE phase and negative within the FE phase. In contrast, a_3 is negative both in the PE and FE phases for the discontinuous FE-PE phase transition. Additionally, a jump in the magnitude of a_3 occurs for this transition [43]. Moreover, a_3 is positive when the nonlinearity originates from the anisotropy of the polarizability. In contrast, ferroelectric relaxors always exhibit a negative a_3 [43]. Therefore, a scaled nonlinear susceptibility can be applied to distinguish several types of dielectric materials.

The aim of this work is to determine the influence of BM doping on the nonlinear dielectric response of PZT–BM ceramics and to identify the mechanisms of the observed nonlinearity. SEM and TOF-SIMS tests were conducted for the ceramic compositions that have not been studied and published before. The correspondence between the chemical composition and the microstructural and electrical features was discussed.

2 Experimental

2.1 Sintering procedure

A two-stage sintering for a series of PZT–BM ceramics was performed at ambient air pressure [3]. At the first stage, PZT 70/30 and BM reference compounds were obtained. The PZT

and BM ceramics were sintered using the standard high-temperature route. The final sintering of PZT was conducted at 1520 K for 4 h. The PZT ceramics were light yellowish in color. Bismuth manganite ceramics were finally sintered at 1173 K for 1 h. The sintered ceramics were hard and graphite-black in color. At the second stage, the PZT 70/30 and the BM ceramics were ground, mixed, and milled at 430 rpm for 6 h. Next, they were pressed into pellets and used for the synthesis of $(1-x)$ PZT– x BM compounds, where $x = 0.02, 0.055, 0.11, 0.15,$ and 0.22 . The PZT–BM ceramics were sintered at 1420 K, for 3 h, under ambient air pressure. The obtained ceramics were hard and brown to black in color. The ceramic pellets were cut to prepare parallelepiped-shaped samples. Silver paste was applied for electrodes.

2.2 Scanning electron microscopy

The ceramic samples were cleaved or fractured ex situ and polished with diamond paste, grade 2000. Chemical composition and homogeneity tests were conducted with the use of a scanning microscope JSM-5410 equipped with energy dispersion X-ray spectrometer (EDS with Si(Li) X-ray detector). The microanalysis was performed with ISIS-300SEMQuant program. Testing was performed on polished ceramic surfaces with an area of $70 \times 50 \mu\text{m}^2$. The uncertainty of the element concentration estimation was lower than 2 at%.

2.3 Time of flight secondary ion mass spectrometry

Time of flight–secondary ion mass spectrometry (TOF–SIMS) measurements were carried out with the use of a TOF–SIMS 5 (ION–TOF GmbH, Munster, Germany) reflection-type spectrometer, equipped with a bismuth liquid metal ion gun. Positive mass spectra and distribution maps for selected ions were collected by rastering the ion beam across predetermined areas with a size of $50 \times 50 \mu\text{m}^2$. The studies were performed at room temperature in ultra-high vacuum conditions ($\sim 5 \cdot 10^{-9}$ mbar). Sample surface contamination was removed by using a DC current bismuth ion beam treatment. To obtain distribution maps with good lateral resolution, the measurements were performed in the fast imaging mode ($I(\text{Bi}^+) = 0.15$ pA). The analysis for the studied ceramics was carried out using SurfaceLab6 software.

2.4 Linear and nonlinear dielectric susceptibility

The real χ_1' and imaginary χ_1'' parts of the linear dielectric susceptibility were measured using an Agilent E4980A Precision LCR Meter. A driving electric field with an amplitude of $E = 10$ V cm^{-1} and frequency from 21 Hz to 1 MHz was applied. The measurements were carried out for both cooling and heating runs at a rate of $dT/dt = 2$ K min^{-1} , in the temperature range from 90 to 670 K. Next, a simultaneous

measurement of the linear and nonlinear dielectric susceptibilities was conducted using an original experimental setup [44]. A driving electric field with an amplitude of $E = 100 \text{ V cm}^{-1}$ at frequencies ranging from 37 to 1000 Hz was applied. The measurements were carried out for both cooling and heating runs at a rate of $dT/dt = 1 \text{ K min}^{-1}$. The high magnitude of the electric conductivity for the studied samples enforced the high temperature limit for the nonlinear measurement. Temperature management was performed using a LakeShore 335 temperature controller. The electrical measurements were conducted both in nitrogen and helium atmospheres.

3 Results and discussion

3.1 Scanning electron microscopy

Ceramic grains with dimensions of the order of 2–10 μm have been observed [2, 3, 27]. The nominal composition and nominal (Pb:Bi):(Zr:Ti:Mn) ratio and those estimated from the EDS test are shown in Table 1. The nominal composition of ABO_3 perovskite equals 20:20:60 at%. However, the determination of the light mass oxygen atom content remains uncertain when the EDS method is applied. Hence, we refer to the concentration ratio of the metallic elements as an indicator of the real composition. In the case of the $(1-x)$ PZT- x BM compounds, we assumed that Bi ions replaced Pb ions in the A sublattice and that Mn ions were built into the B sublattice. Therefore, we expected the ratio $(\text{A}':\text{A}''):(\text{B}':\text{B}'':\text{B}''') = 50:50$ for the atoms in the A and B sublattices, respectively. The measured ratio Pb:Zr:Ti = (48.4:0):(34.8:16.8:0) = 48.4:51.6 estimated for PZT ceramics was close to the nominal value 50:(35:15:0). The measured concentration of the Bi and Mn atoms increased when the nominal BM content increased. However, fluctuation in the real concentration occurred within the accuracy limit. It should be noted that in the case of the slightly doped ceramics, $x = 2$ at%, the Bi and Mn concentrations were not estimated because the Pb line in the spectrum markedly overlapped the Bi line and the Mn line, had a low

magnitude, and did not sufficiently protrude from the background.

The compositional features obtained from the SEM test of the BM ceramics have been reported in a previous paper [27]. The average composition (in at.%) was estimated: 48 ± 3 for Bi and 52 ± 3 for Mn. Such a result was satisfactorily close to the nominal composition 50:50 of the elements introduced for sintering. However, the local concentration determined for individual grains corresponds to the two thermodynamically stable phases of this material, $\text{Bi}_{12}\text{MnO}_{20}$ and BiMn_2O_5 , when the bismuth manganite synthesis was performed at ambient pressure conditions [25, 27]. For instance, a Bi:Mn ratio equal to 37:63 was measured for the main phase, which resembled the BiMn_2O_5 composition. On the other hand, a ratio of Bi:Mn equal to 82:18 was estimated for the precipitation, which was dominated by Bi element. Such a composition would correspond to the $\text{Bi}_{12}\text{MnO}_{20}$ phase.

3.2 Time of flight–secondary ion mass spectrometry

Further surface microanalysis was performed with the use of a TOF-SIMS spectrometer. The measurements allowed one to obtain high lateral resolution maps for the Pb^+ , Zr^+ , Ti^+ , and Mn^+ ion distributions. (*Note:* symbol of metal, Me^+ , only denotes the positive charge of an ion released from the surface and not the valence state of an ion bounded in the crystal lattice.) The distribution maps for the Pb^+ , Zr^+ , Ti^+ , and Mn^+ ions and overlay maps, which show correlation between paired ions, are combined in Fig. 1. The results are discussed in terms of surface morphology and chemical microstructure. It should be noted that a negligible amount of the Mn^+ ions was detected in the PZT surface; such an amount is generally irrelevant remembering that the detection limits of TOF-SIMS are high. In the case of the BM ceramics, negligible amounts of Pb^+ , Zr^+ , and Ti^+ ions were detected. To systematically compile the data, these maps were placed in Fig. 1: see dark, blackish contrast in (a2), (a3), (g1), (g2), and (g3) images. The analysis of the morphology of PZT and $(1-x)$ PZT- x BM ceramics is based on analysis of the distribution maps of Pb^+

Table 1 Nominal content of BM, x , nominal composition of $(1-x)$ PZT- x BM compounds, nominal (Pb:Bi):(Zr:Ti:Mn) ratio, measured ratio, $(\text{A}':\text{A}''):(\text{B}':\text{B}'':\text{B}''')$, and A:B ratio estimated from the EDS test

x (at%)	Nominal composition	Nominal ratio (at%) (Pb:Bi):(Zr:Ti:Mn)	Measured ratio (at%) (Pb:Bi):(Zr:Ti:Mn)	Measured ratio A:B	Reference
0	$\text{Pb}(\text{Zr}_{0.70}\text{Ti}_{0.30})\text{O}_3$	(50:0):(35:15:0)	(48.4:0):(34.8:16.8:0)	48.4:51.6	[2]
2	$0.98\text{Pb}(\text{Zr}_{0.70}\text{Ti}_{0.30})\text{O}_3-0.02\text{BiMnO}_3$	(49:1):(34.3:14.7:1.0)	(51.6:—):(35.7:12.7:—)	51.6:48.4	this work
5.5	$0.945\text{Pb}(\text{Zr}_{0.70}\text{Ti}_{0.30})\text{O}_3-0.055\text{BiMnO}_3$	(47.2:2.8):(33.6:13.6:2.8)	(46.2:3.7):(32.6:16.9:0.6)	49.9:50.1	[2]
11	$0.89\text{Pb}(\text{Zr}_{0.70}\text{Ti}_{0.30})\text{O}_3-0.11\text{BiMnO}_3$	(44.5:5.5):(31.2:13.3:5.5)	(45.9:4.5):(31.2:12.7:5.7)	50.4:49.6	[2]
15	$0.85\text{Pb}(\text{Zr}_{0.70}\text{Ti}_{0.30})\text{O}_3-0.15\text{BiMnO}_3$	(42.5:7.5):(29.8:12.7:7.5)	(42.1:6.0):(32.6:11.4:7.9)	48.1:51.9	this work
22	$0.78\text{Pb}(\text{Zr}_{0.70}\text{Ti}_{0.30})\text{O}_3-0.22\text{BiMnO}_3$	(39:11):(27.3:11.7:11.0)	(46.1:7.9):(27.1:10.9:8.0)	54.0:46.0	this work

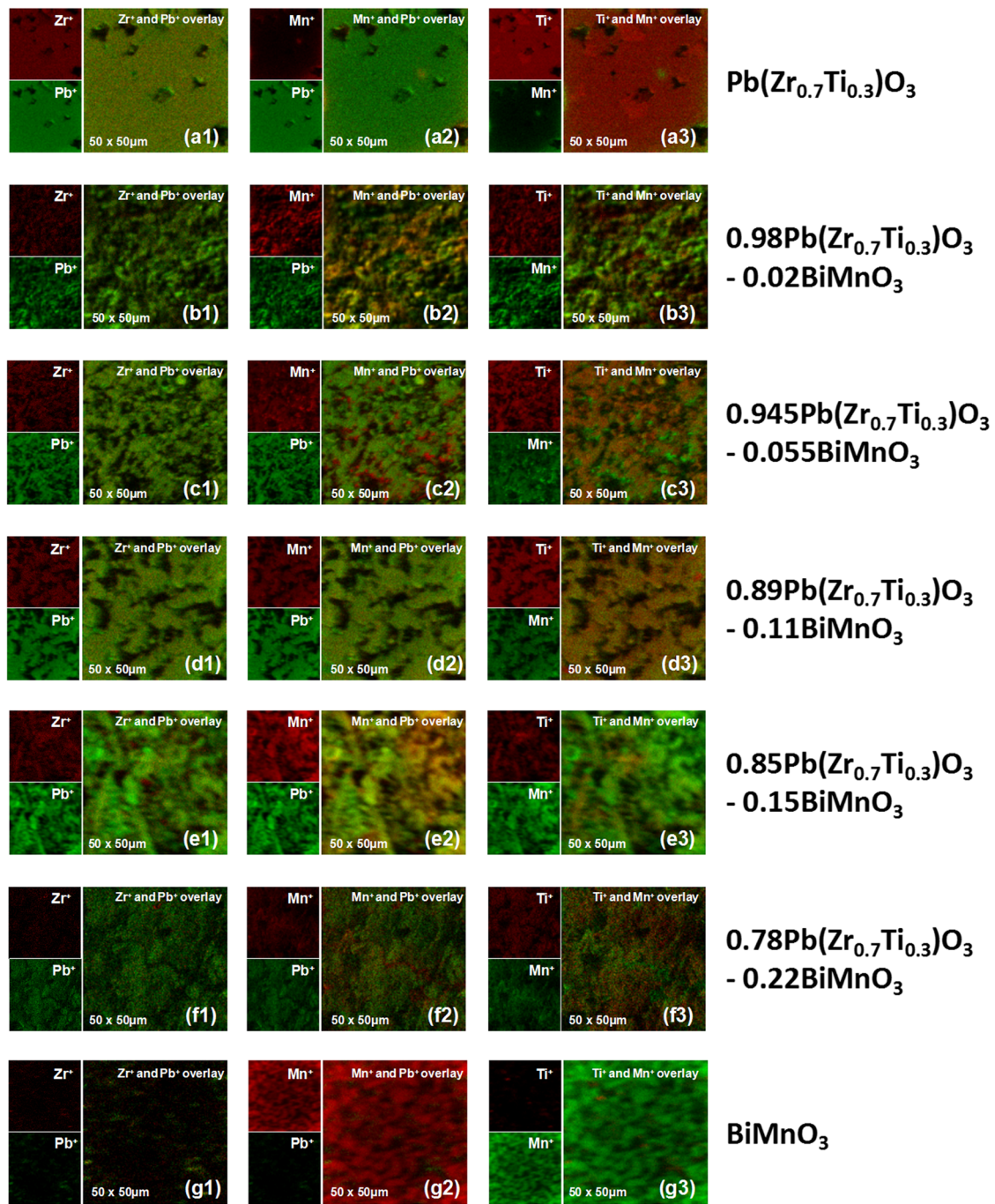


Fig. 1 Distribution maps and their overlays obtained from the $50 \times 50 \mu\text{m}^2$ areas of $(1-x)$ PZT- x BM series for: $x = 0$ (PZT) (a), $x = 0.02$ (b), $x = 0.055$ (c), $x = 0.11$ (d), $x = 0.15$ (e), $x = 0.22$ (f), and $x = 1$ (BM) (g). The first column (1) represents the distribution maps of Zr^+

(red) and Pb^+ (green) ions together with their overlays, the second column (2) Mn^+ (red) and Pb^+ (green), and the third column (3) Ti^+ (red) and Mn^+ (green)

and Zr^+ ions, which are the main components that reflect the structure of the ceramic surface. The distribution of Mn^+ ions was taken into account for the analysis of the morphology of BM ceramics.

Distribution maps for the $(1-x)$ PZT- x BM composites indicate that the morphology of the samples, that is, both the

grain size and porosity, varied dependably on the chemical composition of the samples. The surface of the PZT sample is almost homogeneous with a small number of pores visible in Fig. 1(a1). For $(1-x)$ PZT- x BM compounds, the size of the grains increased with the amount of the substituent, when $x = 0.02$ – 0.15 . The morphology of the surface became grainy

for a low substitution level, $x = 0.02$ and $x = 0.055$ (Fig. 1(b1) and (c1)). However, the grain sizes were relatively small (of the order of several micrometers). In the case of $x = 0.11$ and $x = 0.15$ (Fig. 1(d1) and (e1)) substitution, the other graininess of the surfaces is visible. Grains form agglomerates with a size of the order of tens of micrometers. In the case of $x = 0.15$ substitution, a mixture of grains of different sizes is visible, but the overall morphology is similar to that found for samples containing smaller amounts of Mn constituents. In contrast, the morphology changed for the highest substitution, $x = 0.22$ (Fig. 1(f1)). The surface of this sample became more homogeneous, and pores were not observed. The distribution map of Mn^{+} ions obtained for the BM sample (Fig. 1(g3)) indicates that the surface exhibits a homogenous, densely packed grainy structure, which does not contain pores. Chemical correlations within the microstructure of the ceramic $(1-x)$ PZT- x BM composite constituents have been analyzed based on the overlay maps for particular pairs of ions shown in Fig. 1 (Zr^{+}/Pb^{+} , Mn^{+}/Pb^{+} , and Ti^{+}/Mn^{+}). Homogeneity of the PZT is deduced herein only for the Zr^{+}/Pb^{+} (Fig. 1(a1)) overlay map. For the PZT ceramics with BM substitution, the analysis includes relative changes in the chemical composition of the entire $(1-x)$ PZT- x BM compound. The PZT-based phases were analyzed in terms of overlay maps for the Zr^{+} and Pb^{+} ions (Fig. 1(b1-f1)). The results indicate that for the BM substitution from $x = 0.02$ to $x = 0.11$, the PZT matrix is practically uniform, with a small increase in Pb content in each grain (see increased intensity for Pb^{+} ions in Fig. 1(b1, c1, d1)). For the $x = 0.15$ and $x = 0.22$ compositions, Zr^{+} precipitation can be observed (see red spots in Fig. 1(e1, f1)).

A complex distribution occurred for the Mn^{+} ions. Mn^{+} ions showed a tendency for separation for all $(1-x)$ PZT- x BM compositions, which can be observed as a contrast and spots in overlay maps combined in the second and third columns in Fig. 1. For a small BM content, $x = 0.02$ (Fig. 1(b2)), the Mn^{+} was distributed similarly as the Pb^{+} and Zr^{+} ions. However, relatively large areas with lower Mn (red) and higher Pb (green) amounts can be discerned in the overlay map. For $x = 0.055$, part of the Mn^{+} ions is uniformly distributed in the PZT-BM matrix. However, another part of Mn^{+} appeared in the form of a precipitate at grain boundaries (Fig. 1(c2)). In the case of higher substitution of the BM phase, $x = 0.11$, all ions were uniformly distributed in the ceramic surface (Fig. 1(d2)). The overlay maps obtained for $x = 0.15$ indicate that ions are present in the entire $(1-x)$ PZT- x BM. However, part of the analyzed area is richer in Mn^{+} . Two tendencies occur for the substitution $x = 0.22$. One relates to a uniform distribution of Mn^{+} ions, and the second corresponds to the Mn^{+} precipitations (Fig. 1(f2)).

The overlay maps for Ti^{+} with Mn^{+} , shown in the third column in Fig. 1, exhibit Ti^{+} ions that are uniformly distributed within grain agglomerates. Additionally, the Ti^{+} ions are also separated in the vicinity of pores for ceramics with a low

BM content, $x = 0.02$, $x = 0.055$, and $x = 0.11$ (Fig. 1(b3, c3, d3)). A high amount of Ti^{+} ions was precipitated on the grain boundaries for the 0.78 PZT-0.22 BM ceramics (Fig. 1(g3)).

3.3 Linear and nonlinear dielectric susceptibility

The real, χ_1' , and imaginary, χ_1'' , parts of the linear dielectric susceptibility temperature dependences for the PZT 70/30 and BM reference ceramics and the PZT-BM composites are shown in Fig. 2. The dielectric dispersion of χ_1' and χ_1'' occurs for all ceramics in a wide temperature range.

The PZT 70/30 sample exhibits a sharp $\chi_1'(T)$ peak, typical for the discontinuous ferroelectric phase transition at ~ 610 K. The phase transition temperature, T_{FE-PE} , coincides with the results obtained from the XRD test [3, 16, 45]. The maximum value for the susceptibility decreases from $\sim 46,000$ to $\sim 16,000$ when the measuring frequency increases from 21 Hz to 1 MHz. Moreover, a weak frequency dependence of the position of the temperature peak in $\chi_1'(T)$ was detected. Note that for low frequencies and close to the high temperature limit, the dielectric susceptibility increases with temperature within the paraelectric phase. The second reference ceramic, BM, shows a significantly frequency-dependent $\chi_1'(T)$ anomaly. It shifts from 283 to 470 K when the frequency increases from 21 Hz to 1 MHz. The magnitude of this anomaly is approximately six times lower in comparison to the anomaly in the PZT sample. The addition of the BM compound to the PZT matrix markedly affects the dielectric features of the PZT. The increase in the BM content in the ceramics induces a broadening of the main susceptibility peak and a shift of the peak position toward the lower temperature range. Moreover, the electric probing field frequency markedly influenced the temperature of the χ_1' peak position, $T_{\chi_1'_{max}}$ (see Fig. 3).

Table 2 shows the estimated shift in the temperature peak position per decade of frequency, $\Delta T / \Delta \log(f) = [T_{\chi_1'_{max}}(1 \text{ MHz}) - T_{\chi_1'_{max}}(46 \text{ Hz})] / [\log(1 \text{ MHz}) - \log(46 \text{ Hz})]$. One notices that the shift magnitude increases from ~ 0.4 to ~ 5 K per frequency decade when the BM content increases from 0 to 11%. A shift with a much larger magnitude occurred for BM contents of 0.15 and 0.22%: ~ 46 and ~ 49 K per frequency decade, respectively. The χ_1' value in the peak, measured at low frequency $f = 21$ Hz, increases from $\sim 1 \cdot 10^4$ to $\sim 3 \cdot 10^4$ when the content of BM compound increases in the PZT-BM ceramics. The observed rise of χ_1' in the temperature range above the peak position temperature originates from a contribution from thermally generated charge carriers to the measured effective dielectric susceptibility.

The giant values of $\chi_1''(T)$ also indicate a high concentration of electric charge carriers. The high temperature peak anomaly in the $\chi_1''(T)$ dependences for the PZT sample and for the ceramics with $x \leq 0.11$ corresponds to the peak of χ_1' . $\chi_1''(T)$ for the 0.85 PZT-0.15 BM sample exhibits a weak bump that is visible at high frequencies. A high electric

Fig. 2 Temperature dependences of the real and imaginary part of the linear dielectric susceptibility for PZT, $(1-x)$ PZT- x BM, and BM ceramic samples, where $x = 0.02, 0.055, 0.11, 0.15,$ and 0.22

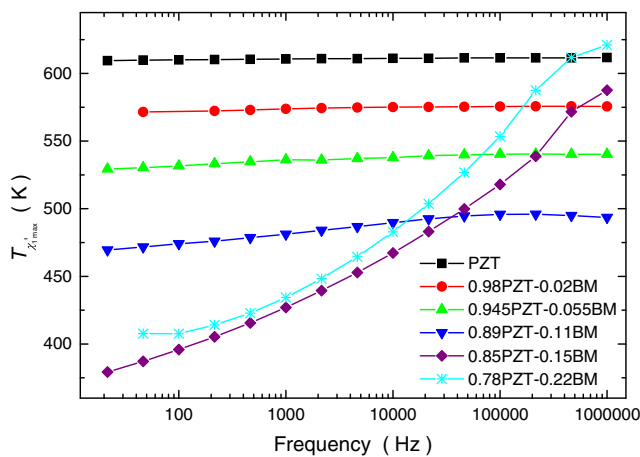
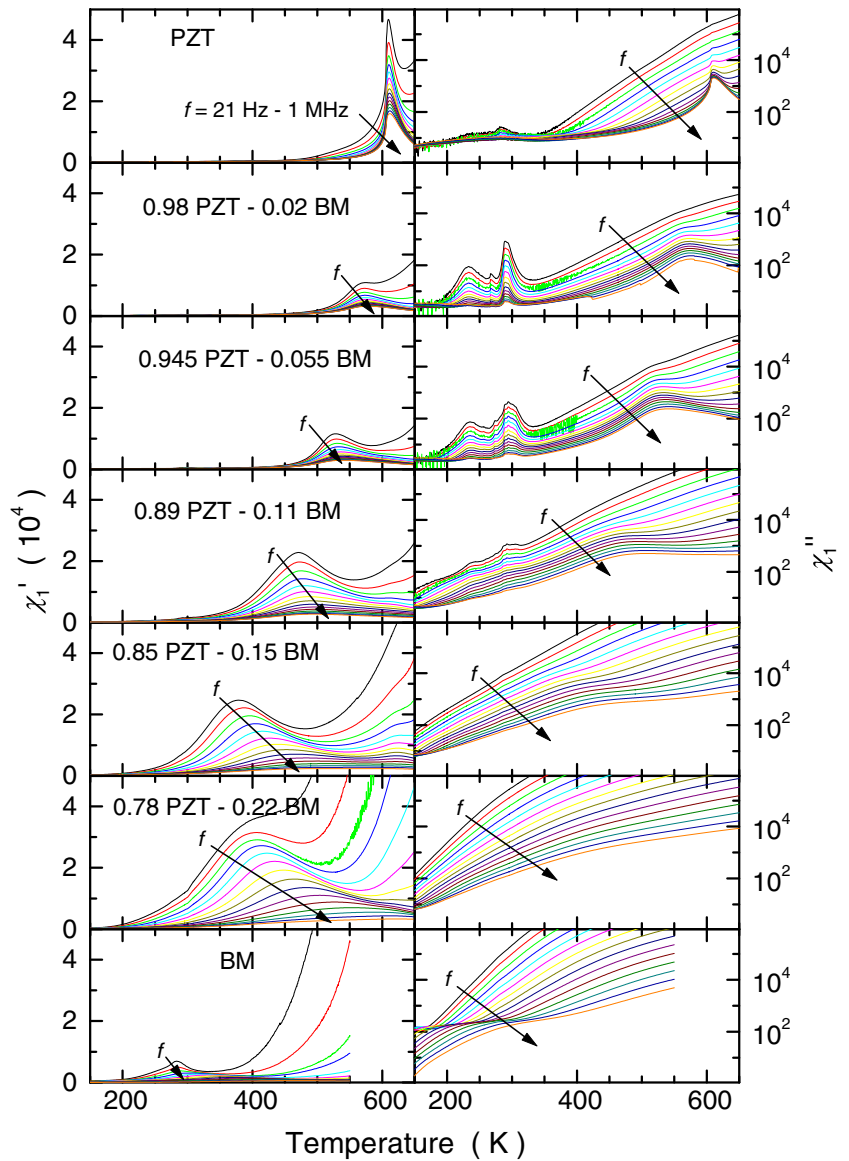


Fig. 3 Frequency dependence of the temperature of the χ_1' peak position, $T_{\chi_1' \max}$, for the $(1-x)$ PZT- x BM composite and PZT ceramics

conductivity contribution overlaps this anomaly at the low frequency limit. In turn, for the 0.78 PZT – 0.22 BM ceramics, the frequency-dependent imaginary part of the susceptibility increases monotonically with temperature. There are additional anomalies in the $\chi_1''(T)$ dependence in the low temperature range in the case of a low BM concentration, $x \leq 0.11$. The occurrence of the bump peak centered at ~ 230 K and the

Table 2 The estimated shift of the χ_1' peak position per decade of frequency obtained for the $(1-x)$ PZT- x BM ceramics series

Composition	$\Delta T/\Delta \log(f)$
PZT	0.4309(30)
0.98 PZT-0.02 BM	0.9467(59)
0.945 PZT-0.055 BM	2.288(12)
0.89 PZT-0.11 BM	5.042(23)
0.85 PZT-0.15 BM	46.264(36)
0.78 PZT-0.22 BM	49.230(60)

narrower peak centered at ~ 300 K is independent of the helium and nitrogen atmosphere in the measuring chamber. Therefore, these anomalies cannot be attributed to H_2O contamination of the samples. The bump anomaly can be assigned to the crossover between monoclinic M_B and M_A structures [45]. The origin of the narrower peak, visible at ~ 300 K, remains unknown. It should be noticed that the transition between ferroelectric rhombohedral phases occurs in the vicinity of 350 K [16, 45]. The tiny anomaly detected at 273 K was attributed to the contribution from residual H_2O molecules. We would like to note that the magnitude of this tiny peak was markedly diminished when a dry helium atmosphere was applied.

Figure 4 shows the temperature dependences of the real part of the linear dielectric susceptibility, the real part of the third-order nonlinear dielectric susceptibility all simultaneously measured at $f = 317$ Hz, and the calculated scaled nonlinear susceptibility for the studied ceramics. The linear susceptibility temperature dependences (Fig. 4a) correspond to the data

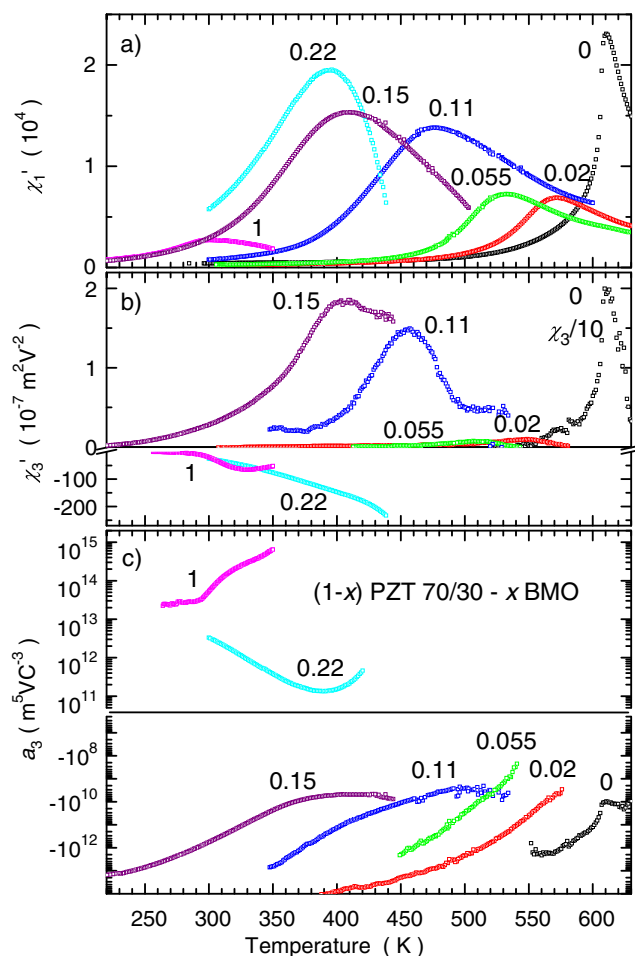


Fig. 4 Temperature dependences of the real part of the linear dielectric susceptibility (a), the real part of the third-order nonlinear dielectric susceptibility (b) and the scaled nonlinear susceptibility (c) measured at $f = 317$ Hz for the $(1-x)$ PZT- x BM ceramics series ($x = 0, 0.02, 0.055, 0.11, 0.15, 0.22$, and 1)

shown in Fig. 2. The values of the third-order susceptibility (Fig. 4b), χ_3' , are positive for the PZT and for the ceramics doped with a low amount of BM ($x \leq 0.15$). $\chi_3'(T)$ for PZT exhibits a sharp asymmetric peak near the phase transition. This $\chi_3'(T)$ temperature dependence, in the vicinity of T_C , is almost discontinuous inside the ferroelectric phase and much steeper in comparison to the dependence inside the paraelectric phase. There are wide anomalies in the $\chi_3'(T)$ dependences visible for the $(1-x)$ PZT- x BM ceramics ($0.02 \leq x \leq 0.15$). The magnitudes of χ_3' , obtained for doping levels of $x = 0.02$ and 0.055, are lower than the magnitudes of χ_3' obtained for ceramics containing a higher amount of BM. This effect corresponds to the tendency of the changes in the χ_1' magnitude. For the case of the sample with the highest BM concentration studied herein, 0.78 PZT-0.22 BM, and for the reference BM sample, a qualitative change in the χ_3' is observed. In contrast to the low-doped samples, the sign of χ_3' is negative over the whole temperature range. Additionally, the magnitudes of χ_3' are at least one order higher than those observed for the low-doped samples. In accordance with Eq. 3, the sign of a_3 is opposite to the sign of χ_3' . Therefore, a_3 (Fig. 4c) is negative for $(1-x)$ PZT- x BM, where $0 \leq x \leq 0.15$. The negative values and step-like anomaly in a_3 obtained for the pure PZT sample indicate the occurrence of a discontinuous PE-FE phase transition near 610 K. The negative values and smooth $a_3(T)$ dependences occur for samples with low BM concentrations ($x = 0.02, 0.055, 0.11, 0.15$), which are characteristic for relaxor materials. In contrast, a quite different feature for a_3 occurs for the highest doped samples, 0.78 PZT-0.22 BM and BM. The a_3 is positive in the whole temperature range. Such a feature can be attributed to the anisotropy of the material polarizability [37]. This anisotropy can result from the occurrence of dipoles created by charges trapped in a double well potential [36, 40]. In $(1-x)$ PZT- x BM, hopping charge transfer between acceptor-type defects, i.e., the $\text{Mn}^{3+}/\text{Mn}^{4+}$, $\text{Ti}^{3+}/\text{Ti}^{4+}$, $\text{Zr}^{3+}/\text{Zr}^{4+}$ ions in the Ti/Zr sublattice, was determined [2, 3]. Hence, we deduce that negative values of χ_3' and thus positive a_3 originate from the occurrence of dipoles created by trapped charges.

In the studied $(1-x)$ PZT- x BM ceramics series, a crossover in electrical features was observed when the BM content increased. Simultaneously, a gradual evolution of the microstructure occurred. Discussion on the correspondence is carried out to the extent that is allowed when macroscopic-scale electrical features and local microscopic structural features are compared.

The PZT ceramic reference samples showed classical ferroelectric properties. One can notice that the FE state relates to the chemical homogeneity of the PZT ceramics deduced from the overlay maps of Zr^+ and Pb^+ ions obtained by the TOF-SIMS test. The homogeneity of the PZT samples has also been proved from a uniform contrast in Zr^+/Pb^+ , Ti^+/Zr^+ , and Ti^+/Pb^+ overlay maps, as presented in a previous paper [3].

For low and intermediate BM contents, $x = 0.02\text{--}0.15$, the relaxor state corresponded to the tendency for the separation or precipitation of the Pb, Ti and Mn ions, which was a distinctive feature in the tested samples, while the Zr exhibited a much more uniform distribution. The overlay maps of Ti^+ with Mn^+ , shown in the third column of the images in Fig. 1, exhibit similar behavior to that reported in a previous paper [3]. Moreover, a nonhomogeneous distribution of Mn ions, as obtained from the TOF-SIMS test, correlates to the XRD test results. It has been shown that the $(1-x)$ PZT- x BM compound should be considered as a structural composite formed of two phases. These phases exhibit features of solid state solutions because Vegard's law was fulfilled for both phases. It has been deduced that one phase was the PZT-based doped with Bi and Mn ions and that the second phase consisted of bismuth-manganite doped with Pb, Ti, and Zr ions [2]. Therefore, chemically and structurally disordered regions form the premise for the occurrence of polar nanoregions, which are responsible for the appearance of the relaxor state [42, 43, 46–48].

The nonhomogeneities observed for the Mn^+ distribution in ceramics with high substitution level, $x = 0.15$ and $x = 0.22$, are of different character. The first ceramics ($x = 0.15$) shows a nonuniform density level for Mn^+ ions in particular areas, e.g., in the vicinity of the boundaries of grain agglomerates. The second ceramics ($x = 0.22$) exhibits a uniform distribution and also an excess of Mn^+ segregated in specific regions. These results also correspond to the occurrence of dipoles, which dominated the dielectric response for the $0.78 \text{Pb}(\text{Zr}_{0.70}\text{Ti}_{0.30})\text{O}_3\text{--}0.22 \text{BiMnO}_3$ and the BM compounds, which was deduced from the positive sign of the scaled nonlinear susceptibility, a_3 . The dipoles originating from the dynamic behavior of trapped charges can be assigned either to polaronic or ionic effects. The occurrence of charge order transfer, $\text{Mn}^{3+}/\text{Mn}^{4+}$, is proposed. Such a conclusion is justified by the results obtained by the XPS test conducted for the BM ceramics [25, 27]. It has been shown that the Mn $2p$ line can be fitted with doublet lines assigned to Mn^{2+} , Mn^{3+} , and Mn^{4+} states and to the contribution of nonidentified defects. Moreover, correspondence of the Mn ion line and the marked broadness of the O $1s$ line was noticed, which indicated the occurrence of oxygen vacancies. The $\text{Mn}^{3+}/\text{Mn}^{4+}$ charge transfer is also consistent with the occurrence of the BiMn_2O_5 phase, which consists of Mn^{3+}O_5 square pyramids and Mn^{4+}O_6 octahedrons. From such a point of view, the polaron hopping enables the dipole-type contribution to give rise to a nonlinear response for all the $(1-x)$ PZT- x BM compositions [8, 9, 17, 21, 22]. The change in sign of the a_3 coefficient in the nonlinear feature originates from the prevailing dipole subsystem in the ceramics for $x = 0.22$ and $x = 1$. Hence, we would like to point out another possible

mechanism for the appearance of dipoles responsible for the changeover from the relaxor state to the dielectric features dominated by a dipole subsystem. We presume that a high content of Mn ions provides a potentially high concentration of dipoles available for the nonlinear response. The conditions for hopping of Mn ions are fulfilled despite the BM and the $0.78 \text{Pb}(\text{Zr}_{0.70}\text{Ti}_{0.30})\text{O}_3\text{--}0.22 \text{BiMnO}_3$ ceramics exhibiting an almost homogeneous distribution of Mn ions, both in the BM phase and the PZT-based phase doped with Mn ions. The defected and locally disordered structure allows connection of the gate model and the occurrence of dipole-like bi-vacancies, $V_{\text{O}}\text{--}V_{\text{B}}$ [46, 49]. We assume that the B-sublattice Mn_{B} ions jumping between potential walls over an energy barrier is possible via a nearest-neighbor oxygen vacancy, V_{O} , to a next-nearest-neighbor B-sublattice vacancy, V_{B} . In the framework of the considered model, the hopping is assigned to the Mn^{4+} ions because of their small radius in comparison to the ionic radii of the Ti^{4+} , Zr^{4+} , Mn^{3+} , and Mn^{2+} ions, for which hopping is less probable [49, 50]. A crossover from dielectric to conductive features was not detected for the ceramics studied herein. It is worth noting that a reversible resistance switching effect between semiconductor and metallic-like states in the BM compound has been induced only by electroformation in the high temperature range not applied in the current studies [27]. It would be noticed that the Mn ion segregation was insufficient for the appearance of the percolation effect.

4 Conclusions

A BM admixture to PZT introduces compositional disorder and a marked amount of trapped charge carriers. The compositional disorder causes a change in the features of the nonlinear electrical response, i.e., a crossover from a typical FE-PE discontinuous phase transition to a relaxor-type subsystem. The a_3 was negative for low BM content ($0 \leq x \leq 0.15$) in the whole temperature range that is specific for the discontinuous ferroelectric phase transitions and for the relaxor behavior. In contrast, the a_3 was positive both for the BM reference and the PZT-BM ceramics when the BM content was high ($x = 0.22$). This feature relates to the dipole subsystem. The dipoles can be attributed either to polaronic or ionic contributions. In both cases, Mn ions can be responsible for the formation of these dipoles. Therefore, when the BM content was increased, the number density of dipoles increased. Hence, when the BM content was high enough, $x \geq 0.22$, the dipole subsystem response dominated the nonlinear features. We note that the measurement of both the magnitude and the sign of χ'_3 enabled the detection of this crossover in the electrical features.

Acknowledgements This research did not receive any specific grant from funding agencies in the public, commercial, or not-for-profit sectors.

Open Access This article is licensed under a Creative Commons Attribution 4.0 International License, which permits use, sharing, adaptation, distribution and reproduction in any medium or format, as long as you give appropriate credit to the original author(s) and the source, provide a link to the Creative Commons licence, and indicate if changes were made. The images or other third party material in this article are included in the article's Creative Commons licence, unless indicated otherwise in a credit line to the material. If material is not included in the article's Creative Commons licence and your intended use is not permitted by statutory regulation or exceeds the permitted use, you will need to obtain permission directly from the copyright holder. To view a copy of this licence, visit <http://creativecommons.org/licenses/by/4.0/>.

References

1. K. Uchino, Politico-engineering—politically—initiated engineering in piezoelectric devices. *SOJ Mater Sci Eng* **1**, 1–10 (2013)
2. A. Molak, R. Bujakiewicz-Korońska, Z. Ujma, A. Leonarska, A.Z. Szeremeta, I. Gruszka, D.M. Nalecz, Electric features of PZT 70/30 – BiMn₂O₅ solid solution ceramics. *J Eur Ceram Soc* **35**, 2513–2522 (2015)
3. A.Z. Szeremeta, S. Pawlus, M. Pilch, K. Balin, A. Leonarska, A. Molak, M. Paluch, Relaxor state and electric relaxations induced by the addition of bi and Mn ions to Pb(Zr_{0.70}Ti_{0.30})O₃ ceramics. *Ceram Int* **43**, 11699–11709 (2017)
4. R. Bujakiewicz-Korońska, Ab initio calculations for the tetragonal PbZr_{0.5}Ti_{0.5}O₃. *Comput Mater Sci* **77**, 399–402 (2013)
5. B. Guiffard, E. Boucher, L. Eyraud, L. Lebrun, D. Guyomar, Influence of donor co-doping by niobium or fluorine on the conductivity of Mn doped and mg doped PZT ceramics. *J Eur Ceram Soc* **25**, 2487–2490 (2005)
6. C. Ang, Z. Yu, L.E. Cross, Oxygen–vacancy–related low–frequency dielectric relaxation and electrical conduction in bi: SrTiO₃. *Phys Rev B* **62**, 228–236 (2000)
7. T. Kamiya, T. Suzuki, T. Tsurumi, M. Daimon, Effects of manganese addition on piezoelectric properties of Pb(Zr_{0.5}Ti_{0.5})O₃. *Jpn J Appl Phys* **31**, 3058–3060 (1992)
8. E. Boucher, B. Guiffard, L. Lebrun, D. Guyomar, Effects of Zr/Ti ratio on structural, dielectric and piezoelectric properties of Mn–And (Mn, F) –doped lead zirconate titanate ceramics. *Ceram Int* **32**, 479–485 (2006)
9. A. Boonchun, M.F. Smith, B. Cherdhirunkorn, S. Limpijumnong, First principles study of Mn impurities in PbTiO₃ and PbZrO₃. *J Appl Phys* **101**, 043521–1–043521–7 (2007)
10. B. Cherdhirunkorn, M.F. Smith, S. Limpijumnong, D.A. Hall, EXAFS study on the site preference of Mn in perovskite structure of PZT ceramics. *Ceram Int* **34**, 727–729 (2008)
11. G. Shirane, K. Suzuki, A. Takeda, Phase transitions in solid solution of PbZrO₃ and PbTiO₃ (II) X-ray study. *J Phys Soc Jpn* **7**, 12–18 (1952)
12. J. Ricote, D.L. Corker, R.W. Whatmore, S.A. Impey, A.M. Glazer, J. Dec, K. Roleder, A TEM and neutron diffraction study of the local structure in the rhombohedral phase of lead zirconate titanate. *J Phys Condens Matter* **10**, 1767–1786 (1998)
13. A. Munoz, J.A. Alonso, M.T. Casais, Martinez–Lope MJ, Martinez JL, Fernandez–Diaz MT. Magnetic structure and properties of BiMn₂O₅ oxide: A neutron diffraction study. *Phys Rev B* **65**, 144423–1–144423–8 (2002)
14. J. Zhang, B. Xu, X.F. Li, K.L. Yao, Z.L. Liu, Origin of the multiferroicity in BiMn₂O₅ from first–principles calculations. *J Magn Magn Mater* **323**, 1599–1605 (2011)
15. A. Leonarska, M. Kądziołka-Gaweł, A.Z. Szeremeta, R. Bujakiewicz-Korońska, A. Kalvane, A. Molak, Electric relaxation and Mn³⁺/Mn⁴⁺ charge transfer in Fe-doped Bi_{1/2}MnO_{2/0}–BiMn₂O₅ structural self-composite. *J Mater Sci* **52**, 2222–2231 (2017)
16. B. Noheda, D.E. Cox, G. Shirane, R. Guo, B. Jones, L.E. Cross, Stability of the monoclinic phase in the ferroelectric perovskite. *Phys Rev B* **63**, 014103–1–014103–9 (2000)
17. G.J. Hu, T. Zhang, J.L. Sun, D.M. Zhu, H.J. Chu, Dielectric relaxation associated with dipolar defect complex in PbZr_xTi_{1–x}O₃. *J Infrared Milim Waves* **28**, 321–324 (2009)
18. C.C. Wang, L.W. Zhang, Polaron relaxation related to localized charge carriers in CaCu₃Ti₄O₁₂. *Appl Phys Lett* **90**, 142905–1–142905–3 (2007)
19. A.A. Bokov, M. Maglione, Z.-G. Ye, Quasi–ferroelectric state in Ba(Ti_{1–x}Zr_x)O₃ relaxor: dielectric spectroscopy evidence. *J Phys Condens Matter* **19**, 092001–1–092001–10 (2007)
20. Levstik A, Filipič C, Bobnar V, Dmrovšek S, Holc J, Kosec M. Polaron conductivity mechanism in 0.5Pb(Zr_{0.575}Ti_{0.425})O₃–0.5Pb(Fe_{2/3}W_{1/3})O₃. *Phys B Condens Matter* 2010;405:4271–4273
21. L. Ni, X.M. Chen, Dielectric relaxations and formation mechanism of giant dielectric constant step in CaCu₃Ti₄O₁₂ ceramics. *Appl Phys Lett* **91**, 122905–1–122905–3 (2007)
22. C.-C. Wang, M.-N. Zhang, K.-B. Xu, G.-J. Wang, Origin of high–temperature relaxor–like behavior in CaCu₃Ti₄O₁₂. *J Appl Phys* **112**, 034109–1–034109–11 (2012)
23. D. Sedmidubsk’y, J. Leitner, O. Beneš, Phase equilibria modeling in Bi₂O₃–SrO–MnO_x system. *Comput Coupling Phase Diagrams Thermochem* **30**, 179–184 (2006)
24. A. Molak, A. Leonarska, A.Z. Szeremeta, Electric current relaxation and resistance switching in non-homogeneous bismuth manganite. *Ferroelectrics* **486**, 161–172 (2015)
25. M. Pilch, A. Molak, J. Koperski, P. Zajdel, Influence of nitrogen flow during sintering of bismuth manganite ceramics on grain morphology and surface disorder. *Phase Transit* **90**, 112–124 (2017)
26. A. Molak, Chemical capacitance proposed for manganite-based ceramics. *Cond Matter Phys* **16**, 31801–1–31801–10 (2013)
27. A. Molak, Z. Ujma, M. Pilch, I. Gruszka, M. Pawelczyk, Resistance switching induced in BiMnO₃ ceramics. *Ferroelectrics* **464**, 59–71 (2014)
28. K.B. Xu, C.C. Wang, M.N. Zhang, G.J. Wang, Y.M. Cui, Polaronic relaxation in La_{0.8}Bi_{0.2}Fe_{0.7}Mn_{0.3}O₃. *Mater Chem Phys* **134**, 499–502 (2012)
29. L. Fang, M. Shen, F. Zheng, Z. Li, J. Yang, Dielectric responses and multirelaxation behaviors of pure and doped CaCu₃Ti₄O₁₂ ceramics. *J Appl Phys* **104**, 064110–1–064110–8 (2008)
30. C.C. Wang, L.W. Zhang, Polaron relaxation related to localized charge carriers in Pr_{1–x}Ca_xMnO₃. *New J Phys* **9**, 210–1–210–10 (2007)
31. G. Wang, C. Wang, S. Huang, C. Lei, X. Sun, T. Li, J. Mei, Polaronic relaxation in Ca₂TiMnO₆ at low temperatures. *Mater Res Bull* **47**, 2692–2695 (2012)
32. S.A. Prosdandeyev, N.M. Teslenko, A.V. Fisenko, Breaking of symmetry of one-electron orbitals at oxygen vacancies in perovskite-type oxides. *J Phys Condens Matter* **5**, 9327–9344 (1993)
33. M. Palcut, J.S. Christensen, K. Wiik, T. Grande, Impurity diffusion of ¹⁴¹Pr in LaMnO₃, LaCoO₃ and LaFeO₃ materials. *Phys Chem Chem Phys* **10**(43), 6544–6552 (2008)
34. K. Funke, R.D. Banhatti, S. Brueckner, C. Cramer, C. Krieger, A. Mandanici, C. Martiny, I. Ross, Ionic motion in materials with disordered structures: Conductivity spectra and the concept of mismatch and relaxation. *Phys Chem Chem Phys* **4**, 3155–3167 (2002)
35. K. Funke, R.D. Banhatti, Ionic motion in materials with disordered structures. *Solid St Ionics* **177**, 1551–1557 (2006)

36. B. Roling, Hopping dynamics of ions and polarons in disordered materials: On the potential of non-linear conductivity spectroscopy. *J Chem Phys* **117**, 1320–1327 (2002)
37. C.J.F. Böttcher, *Theory of Electric Polarization* (Elsevier, Amsterdam, 1973)
38. S. Ikeda, H. Kominami, K. Koyama, Y. Wada, Nonlinear dielectric constant and ferroelectric-to-paraelectric phase transition in copolymers of vinylidene fluoride and trifluoroethylene. *J Appl Phys* **62**, 3339–3342 (1987)
39. A.E. Glazounov, A.K. Tagantsev, Phenomenological model of dynamic nonlinear response of relaxor ferroelectrics. *Phys Rev Lett* **85**(10), 2192–2195 (2000)
40. F. Kremer, A. Schoenhals, *Broadband Dielectric Spectroscopy* (Springer-Verlag, Berlin, 2003)
41. Z. Kutnjak, C. Filipič, R. Pirc, A. Levstik, R. Farhi, M.E. Marssi, Slow dynamics and ergodicity breaking in a lanthanum-modified lead zirconate titanate relaxor system. *Phys Rev B* **59**, 294–301 (1999)
42. S. Miga, J. Dec, A. Molak, M. Koralewski, Barium doping-induced polar nanoregions in lead germanate single crystal. *Phase Transit* **81**, 1133–1140 (2008)
43. Miga S, Dec J, Kleemann W. Non-linear Dielectric Response of Ferroelectrics, Relaxors and Dipolar Glasses. In: *Ferroelectrics - Characterization and Modeling*. Editor: Lallart M. Rijeka: InTech; 2011
44. S. Miga, J. Dec, W. Kleemann, Computer-controlled susceptometer for investigating the linear and non-linear dielectric response. *Rev Sci Instrum* **78**, 033902–1–033902–7 (2007)
45. N. Zhang, H. Yokota, A.M. Glazer, Z. Ren, D.A. Keen, D.S. Keeble, P.A. Thomas, Z.-G. Ye, The missing boundary in the phase diagram of $\text{PbZr}_{1-x}\text{Ti}_x\text{O}_3$. *Nat Commun* **5**, 5231–1–5231–9 (2014)
46. G.A. Samara, L.A. Boatner, Ferroelectric-to-relaxor crossover and oxygen vacancy hopping in the compositionally disordered perovskites $\text{KTa}_{1-x}\text{Nb}_x\text{O}_3\text{:Ca}$. *Phys Rev B* **61**, 3889–3896 (2000)
47. J.F. Scott, Absence of true critical exponents in relaxor ferroelectrics: The case for defect dynamics. *J Phys Condens Matter* **18**, 7123–7134 (2006)
48. V. Westphal, W. Kleemann, M.D. Glinchuk, Diffuse phase transitions and random-field-induced domain states of the "Relaxor" ferroelectric $\text{PbMg}_{1/3}\text{Nb}_{2/3}\text{O}_3$. *Phys Rev Lett* **68**(6), 847–850 (1992)
49. A. Molak, M. Paluch, S. Pawlus, Electrical properties of $\text{Pb}(\text{Mn}_{1/3}\text{Nb}_{2/3})\text{O}_3$ ceramics under hydrostatic pressure: Relaxation dynamics and its relation to the subsystem of defects. *Phys Rev B* **78**, 134207–1–134207–13 (2008)
50. Kawamura J, Asayama R, Kuwata N, Kamishima O. In: *Physics of Solid State Ionics*. Editor: Sakuma T, Takahashi H. Kerala, India: Res Sighpost; 2006

Publisher's note Springer Nature remains neutral with regard to jurisdictional claims in published maps and institutional affiliations.